Journal of Organometallic Chemistry 696 (2011) 1432–1440

Contents lists available at ScienceDirect

Journal of Organometallic Chemistry

journal homepage: www.elsevier.com/locate/jorganchem

New osmium cluster compounds containing the heterocyclic ligand 2,3-bis-(diphenylphosphino)quinoxaline (dppq): Ligand isomerization and crystal structures of dppq, the isomeric clusters $Os_3(CO)_{10}$(dppq), and $HOs_3(CO)_9[\mu$-2,3-PhP(η^1-C_6H_4)(Ph_2P)quinoxaline]

Sean W. Hunt [a], Li Yang [a], Xiaoping Wang [b], Michael G. Richmond [a,*]

[a] Department of Chemistry, University of North Texas, Denton, TX 76203, United States
[b] Neutron Scattering Science Division, Oak Ridge National Laboratory, Oak Ridge, TN 37831, United States

ARTICLE INFO

Article history:
Received 27 December 2010
Accepted 11 January 2011

Keywords:
Osmium clusters
Diphosphine isomerization
P–C bond activation
Crystallography
Redox properties

ABSTRACT

Treatment of the labile cluster 1,2-$Os_3(CO)_{10}(MeCN)_2$ (**1**) with the diphosphine ligand 2,3-bis(diphenylphosphino)quinoxaline (dppq) at room temperature affords 1,2-$Os_3(CO)_{10}$(dppq) (**2b**) as the kinetic product of ligand substitution in 84% yield. **2b** isomerizes to the thermodynamically more stable dppq-chelated cluster 1,1-$Os_3(CO)_{10}$(dppq) (**2c**) as the sole observable product under CO at temperatures below 358 K. The kinetics for the conversion of **2b** → **2c** have been investigated by NMR spectroscopy in $CDCl_3$ over the temperature range 323–353 K, and the reaction was found to exhibit a rate law that is first order in **2b**. The calculated activation parameters [$\Delta H^{\neq} = 25.4(4)$ kcal/mol; $\Delta S^{\neq} = -3(1)$ eu] support an intramolecular isomerization scenario, one that involves the migration of phosphine and CO groups about the cluster polyhedron. The disposition of the dppq ligand in the isomeric $Os_3(CO)_{10}$(dppq) clusters has been established by X-ray crystallography and ^{31}P NMR spectroscopy. Photolysis of **2c** at 366 nm leads to CO loss and ortho metalation of one of the aryl groups on the Ph_2P moiety to furnish the hydride cluster $HOs_3(CO)_9[\mu$-PhP(η^1-C_6H_4)(Ph_2P)quinoxaline] (**3**). The isomerization behavior exhibited by **2b** follows that of related diphosphine-substituted Os_3 clusters prepared by us.

1. Introduction

The reactivity of a wide variety of ligands at the activated cluster 1,2-$Os_3(CO)_{10}(MeCN)_2$ (**1**) has been intensely explored over the years. Of the many different classes of ligands examined, diphosphine ligands have received extensive attention. These ligands have been thoroughly investigated with respect to 1) the coordination mode adopted by the ancillary diphosphine at the cluster polyhedron, 2) metal-directed bond activation of the ligand as a route to unusual phosphido- and phosphinidene-capped clusters, and 3) the dynamical properties associated with the fluxional behavior of the ancillary CO and diphosphine ligands [1]. In the case of vicinal diphosphine ligands that possess a rigid backbone, the formal displacement of the MeCN ligands in **1** typically proceeds with the formation of the bridging and/or chelating diphosphine isomers of $Os_3(CO)_{10}$(P–P). The stereochemistry exhibited by the decacarbonyl product depends upon the nature of the diphosphine ligand, with the chelating diphosphine isomer serving as the thermodynamically more stable form of the cluster.

The reaction between **1** and the diphosphine ligands (Z)-$Ph_2PCH=CHPPh_2$ (dppen) [2], 4,5-bis(diphenylphosphino)-4-cyclopentene-1,3-dione (bpcd) [3], 2,3-bis(diphenylphosphino)-N-*p*-tolylmaleimide (bmi) [4], 2-(ferrocenylidene)-4,5-bis (diphenylphosphino)-4-cyclopentene-1,3-dione (fbpcd) [5], 3,4-bis(diphenylphosphino)-5-methoxy-2(5H)-furanone (bmf), and 1,2-bis(diphenylphosphino)benzene (dppbz) has been explored by us, as part of our interest in the coordinative flexibility and ligand activation of these and related ligands at polynuclear clusters. The structures of these particular diphosphine ligands are depicted in Scheme 1. All six pnictogen ligands react with **1** to furnish initially the corresponding bridged clusters 1,2-$Os_3(CO)_{10}$(P–P), which are not stable and readily isomerize to the chelated 1,1-$Os_3(CO)_{10}$(P–P) isomers upon heating [6]. These isomerizations are unaffected by trapping ligands, and each reaction displays a rate law that is first order in starting cluster. Mechanistically speaking, a non-dissociative, unimolecular process involving the migration of phosphorus and CO groups about the cluster polyhedron is in keeping with the kinetic data

* Corresponding author. Tel.: +1 940 565 3548; fax: +1 940 565 4318.
E-mail address: cobalt@unt.edu (M.G. Richmond).

0022-328X/$ – see front matter © 2011 Elsevier B.V. All rights reserved.
doi:10.1016/j.jorganchem.2011.01.019

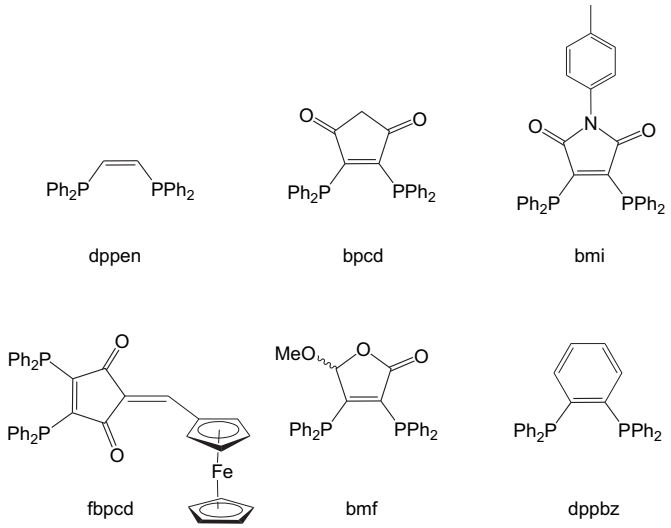

Scheme 1.

and the Eyring activation parameters. DFT calculations on the rearrangement of bridged-to-chelated isomers have verified a merry-go-round exchange of one phosphine and two CO groups [7]. Here the concerted permutation of the three migrating ligands parallels the exchange scheme originally postulated by Cotton over forty years ago for CO migration about the Co–Co vectors in $Co_4(CO)_{12}$ [8].

The rigid diphosphine ligand 2,3-bis(*tert*-butylmethylphosphino)quinoxaline (Quinox-P), which was first prepared by Imamoto et al. [9], has been employed as a chiral auxiliary in asymmetric hydrogenation and C–C bond forming reactions [10]. The redox properties of several d^6 and d^8 mononuclear Quinox-P-substituted compounds have been recently investigated by Kaim et al., and the electron-withdrawing properties of the quinoxaline platform verified by spectroelectrochemical and epr measurements [11]. The observation of site-localized radical anions on the quinoxaline heterocycle confirms the ability of this diphosphine to function as an electron reservoir in electron-transfer reactions.

Given the current interest in the Quinox-P ligand, coupled with the absence of any reports on the reactivity of this genre of diphosphine with polynuclear compounds, we wished to explore the substitution chemistry of the Quniox-P analogue 2,3-bis(diphenylphosphino)quinoxaline (dppq). The Ph_2P-substituted derivative more closely matches those ligand systems already explored by us, and this commonality will facilitate a reactivity comparison of the different ligand systems as a function of the platform that tethers the Ph_2P moieties. Herein we report our results on the reaction between $Os_3(CO)_{10}(MeCN)_2$ and dppq, which affords the bridged and chelated clusters $Os_3(CO)_{10}$(dppq) (**2b** and **2c**) depending upon the reaction conditions. Near-UV photolysis of **2c** leads to CO loss and rapid ortho metalation of one of the ancillary phenyl groups to furnish the corresponding hydride cluster $HOs_3(CO)_9[\mu\text{-}PhP(\eta^1\text{-}C_6H_4)(Ph_2P)$quinoxaline] (**3**). The redox properties of the dppq ligand and clusters **2b** and **2c** have also been examined by cyclic voltammetry, and these data are discussed with respect to the HOMO and LUMO levels computed by DFT calculations.

2. Experimental

2.1. General methods

Cluster **1** was prepared from $Os_3(CO)_{12}$, Me_3NO, and MeCN [12], while the parent cluster $Os_3(CO)_{12}$ was synthesized from OsO_4 and CO [13]. The dppq ligand employed in our studies was synthesized from 2,3-dichloroquinoxaline and Ph_2PH, as described in detail below. The OsO_4 was purchased from Engelhard Chemical Co., and the chemicals $Me_3NO\cdot xH_2O$, 2,3-dichloroquinoxaline, Ph_2PH, and BuLi (2.5 M in hexanes) were purchased from Aldrich Chemical Co. The anhydrous Me_3NO employed in our studies was obtained from $Me_3NO\cdot xH_2O$, after the waters of hydration were azeotropically removed under reflux using benzene as a solvent. The molarity of the BuLi was checked immediately before each reaction by titration against diphenylacetic acid [14]. All reaction solvents were distilled from a suitable drying agent under argon or obtained from an Innovative Technology (IT) solvent purification system. When not in use all purified solvents were stored in Schlenk storage vessels equipped with high-vacuum Teflon stopcocks [15]. The photochemical studies were conducted with GE Blacklight bulbs having a maximum output at 366 ± 20 nm. Combustion analyses were performed by Atlantic Microlab, Norcross, GA.

2.2. Instrumentation

The IR spectra were recorded on a Nicolet 6700 FT-IR spectrometer in amalgamated NaCl cells having a 0.1 mm path length, while the quoted ^1H NMR data were recorded at 400 MHz or 500 MHz on Varian VXR-400 and VXR-500 spectrometers, respectively. The ^{31}P NMR spectra were recorded at 202 MHz on the latter spectrometer, and these data were collected in the proton-decoupled mode and are referenced to external H_3PO_4 (85%), whose chemical shift was set at $\delta = 0$.

2.3. Synthesis of the diphosphine ligand dppq

To a 500 mL Schlenk flask containing ca. 125 mL of hexane and 1.0 g (5.6 mmol) of Ph_2PH at −78 °C was added 2.4 mL (5.8 mmol) of 2.4 M BuLi dropwise, with stirring continued for additional 1 h at this temperature. The slurry was allowed to warm to room temperature, after which the hexane and the unreacted BuLi were cannulated away from the precipitated Ph_2PLi. The phosphide was dissolved in ca. 25 mL of THF and the solution was cooled to at −78 °C, after which the phosphide solution was added dropwise to 0.52 g (2.6 mmol) of 2,3-dichloroquinoxaline in 100 mL of THF at the same temperature. Upon completion of the addition phase, stirring was continued overnight with warming to room temperature. The yellow solution was concentrated to dryness and then taken up in ca. 20 mL CH_2Cl_2, followed by extraction with 3×10 mL portions of water, and drying of the organic layer over $MgSO_4$. The desired product was purified by column chromatography over silica gel using CH_2Cl_2 as the eluent. Recrystallization of the crude product from CH_2Cl_2/hexane at 5 °C gave dppq as a hygroscopic yellow solid in 85% yield (1.1 g). ^1H NMR ($CDCl_3$): δ 7.20–7.29 (m, 12H, aryl), 7.30–7.35 (m, 8H, aryl), 7.67 (m, 2H, quinoxaline ring, $J_{AB} = 8.5$ Hz, $J_{AB'} = 1.3$ Hz, $J_{AA'} = 0.7$ Hz), 7.93 (m, 2H, quinoxaline ring, $J_{AB} = 8.5$ Hz, $J_{AB'} = 1.3$ Hz, $J_{BB'} = 6.8$ Hz). ^1H NMR (C_6D_6): δ 7.03 (bm, 14H, aryl meta and para, quinoxaline), 7.51 (m, 8H, aryl ortho), 7.78 (bm, 2H, quinoxaline). ^{31}P NMR ($CDCl_3$): $\delta -10.72$ (s). ^{31}P NMR (C_6D_6): $\delta -9.55$. Anal. Calcd (found) for $C_{32}H_{24}N_2P_2$: C, 77.10 (76.07); H, 4.85 (4.85).

2.4. Synthesis of 1,2-$Os_3(CO)_{10}$(dppq) (**2b**) from 1,2-$Os_3(CO)_{10}(MeCN)_2$ and dppq

To a Schlenk tube under argon was charged 0.15 g (0.16 mmol) of 1,2-$Os_3(CO)_{10}(MeCN)_2$, followed by 50 mL of CH_2Cl_2 via syringe. To this solution was added, in one portion, 88 mg (0.17 mmol) of dppq and the reaction was stirred at room temperature for 1 h. TLC analysis using CH_2Cl_2/hexane (4:1) confirmed the consumption of the starting cluster and the presence of a new spot attributed to the

desired product ($R_f = 0.93$). The solvent was removed under vacuum and the residue chromatographed over silica gel using the aforementioned mobile phase. The crude product was then recrystallized from a 1:1 mixture of hexane/benzene to afford 0.18 g (84% yield) of **2b** as a red–orange solid. IR (CH_2Cl_2): ν(CO) 2089 (s), 2024 (m), 2009 (vs) 1973 (m), 1953 (m) cm^{-1}. ^1H NMR ($CDCl_3$): δ 7.13–7.18 (m, 8H, aryl), 7.19–7.24 (m, 8H, aryl), 7.28–7.32 (m, 4H, aryl), 7.76 (m, 4H, quinoxaline ring). ^1H NMR (C_6D_6): δ 6.86–7.02 (m, 14H, aryl meta and para, quinoxaline), 7.32 (m, 8H, aryl ortho), 7.63 (m, 2H, quinoxaline ring, $J_{AB} = 8.4$ Hz, $J_{AB'} = 1.4$ Hz, $J_{BB'} = 7.0$ Hz) [16]. ^{31}P NMR ($CDCl_3$): δ 4.73 (s). ^{31}P NMR (C_6D_6): δ 4.41 (s). Anal. Calcd (found) for $C_{42}H_{24}N_2O_{10}Os_3P_2 \cdot$benzene: C, 40.39 (39.96); H, 2.12 (2.64).

2.5. Isomerization of **2b** to 1,1-$Os_3(CO)_{10}$(dppq) (**2c**) under CO

To a small Schlenk tube was added 0.10 g (0.074 mmol) of **2b** and 25 mL of toluene, after which the solution was saturated with CO and the vessel sealed. The reaction was heated overnight at 70 °C in a thermostated bath and then analyzed by TLC analysis, which revealed the presence of an orange spot at $R_f = 0.91$ using a 4:1 mixture of CH_2Cl_2/hexane. Cluster **2c** was isolated, as described above for **2b**, and recrystallized in hexane/benzene to afford **2c** in 90% yield (90 mg). IR (CH_2Cl_2): ν(CO) 2093 (s), 2068 (m), 2044 (vs), 2008 (b, vs), 1989 (m), 1976 (m), 1959 (m), 1923 (w) cm^{-1}. ^1H NMR ($CDCl_3$): δ 7.30–7.38 (m, 12H, aryl meta and para), 7.44–7.48 (m, 8H, aryl ortho), 7.95 (m, 2H, quinoxaline ring, $J_{AB} = 8.4$ Hz, $J_{AB'} = 1.2$ Hz, $J_{AA'} = 0.6$ Hz), 8.22 (m, 2H, quinoxaline ring, $J_{AB} = 8.4$ Hz, $J_{AB'} = 1.2$ Hz, $J_{BB'} = 6.7$ Hz). ^1H NMR (C_6D_6): δ 6.94 (bm, 4H, para), 7.02–7.09 (bm, 10H, meta and dppq), 7.68–7.76 (bm, 10H, ortho and dppq). ^{31}P NMR ($CDCl_3$): δ 12.81 (s). ^{31}P NMR (C_6D_6): δ 13.20 (s). Anal. Calcd (found) for $C_{42}H_{24}N_2O_{10}Os_3P_2 \cdot 1/2$benzene: C, 38.90 (38.31); H, 1.94 (2.58).

2.6. Synthesis of $HOs_3(CO)_9[\mu$-2,3-PhP(η^1-C_6H_4)(Ph_2P)quinoxaline] (**3**) from **2c**

0.10 g (0.074 mmol) of **2c** in a small Schlenk tube was treated with 20 mL of toluene and the solution was then subjected to three freeze–pump–thaw degas cycles. The vessel was sealed and irradiated (366 nm) at room temperature for a period of 3 days. The CO that accompanies the formation of **3** was periodically removed by additional freeze–pump–thaw degas cycles, in order to drive the reaction to completion. Following photolysis, the reaction solvent was concentrated under vacuum and the residue was purified by column chromatography, followed by recrystallization using hexane/benzene to give **3** in 88% yield (86 mg) as a yellow–orange solid. IR (CH_2Cl_2): ν(CO) 2082 (vs), 2041 (vs), 2016 (vs), 2001 (m), 1986 (sh, m), 1979 (m), 1965 (m) cm^{-1}. ^1H NMR ($CDCl_3$): δ − 16.26 (t, μ_2-H, $J_{P\text{-}H} = 13$ Hz), 6.97–7.06 (m, 2H), 7.14–7.19 (m, 2H), 7.26–7.29 (m, 3H), 7.36–7.45 (m, 3H), 7.52–7.57 (m, 3H), 7.59–7.64 (m, 2H), 7.73–7.78 (m, 2H), 7.80–7.86 (m, 2H), 8.07–8.12 (m, 2H), 8.15 (bd, 1H, $J = 8.0$ Hz), 8.29 (bt, 1H, $J = 7.5$ Hz). ^1H NMR (C_6D_6): δ − 15.84 (t, μ_2-H, $J_{P\text{-}H} = 13$ Hz), 6.90–7.04 (m, 12H), 7.08 (bt, 1H, $J = 7.5$ Hz), 7.37–7.42 (m, 2H), 7.53 (d, 1H, $J = 5.0$ Hz), 7.59–7.65 (m, 3H), 7.91–7.96 (m, 2H), 8.39 (bm, 1H), 8.70 (t, 1H, $J = 7.5$ Hz). ^{31}P NMR ($CDCl_3$): δ 14.34, (d, $J_{P\text{-}P} = 24$ Hz), 18.95 (d, $J_{P\text{-}P} = 24$ Hz). ^{31}P NMR (C_6D_6): δ 13.60, (d, $J_{P\text{-}P} = 24$ Hz), 17.58 (d, $J_{P\text{-}P} = 24$ Hz). Anal. Calcd (found) for $C_{37}H_{24}O_{11}Os_3P_2$: C, 37.27 (37.10); H, 1.83 (1.92).

2.7. Kinetic measurements

The conversion of **2b** → **2c** was investigated by either ^{31}P or ^1H NMR spectroscopy in 5 mm NMR tubes that were equipped with a J-Young valve. Each sample was freshly prepared and immediately subjected to three freeze–pump–thaw degas cycles prior to the admission of CO (1 atm). The NMR samples were heated in an external VWR constant temperature bath at the desired temperature, whose value is assumed to be accurate within ±0.5 K of the quoted temperature. The relative molar ratio of the bridging and chelating isomers of **2** was calculated based on the integral value associated with the ^{31}P singlet of each isomer, and the first-order rate constants were determined by graphical analysis by measuring the consumption of the bridging isomer as a function of time. In the case of the ^1H NMR experiment, changes in the cluster composition were determined by integrating the different quinoxaline hydrogens of **2b** relative to a known amount of ferrocene, which was employed as an internal standard. The activation parameters for the isomerization reaction were calculated from a plot of $\ln(k/T)$ versus T^{-1} [17], with the error limits representing the deviation of the data points about the least-squares line of the Eyring plot.

2.8. Electrochemical data

The reported cyclic voltammetry (CV) data were recorded on a PAR Model 273 potentiostat/galvanostat, equipped with positive feedback circuitry to compensate for *i*R drop. The CVs were recorded under oxygen- and moisture-free conditions in a homemade three-electrode cell. A platinum disk was utilized as the working and auxiliary electrode, and the reference electrode utilized a silver wire as a quasi-reference electrode, with the reported potential data standardized against the formal potential of Cp_2Fe/Cp_2Fe^+ redox couple (external), taken to have $E_{1/2} = 0.31$ V [18].

2.9. X-ray crystallography

Single crystals of dppq, **2b**, and **2c**·CH_2Cl_2 suitable for diffraction analysis were grown from CH_2Cl_2/hexane at 5 °C, while the X-ray quality crystals of **3**·2$CDCl_3$ were obtained by the slow evaporation of $CDCl_3$ from an NMR tubing containing the cluster **3**. The X-ray data were collected on an APEX II CCD-based diffractometer at 100 (2) K. The frames were integrated with the available APEX2 software package using a narrow-frame algorithm [19], and the structures were solved and refined using the SHELXTL program package [20]. Each molecular structure was checked using PLATON [21], and all non-hydrogen atoms were refined anisotropically unless otherwise noted. Absorption corrections were applied to all four compounds using SADABS [22]. The location of the bridging hydride ligand in **3**·2$CDCl_3$ was determined with the aid of XHYDEX [23], and the hydride group was allowed to ride on the attached Os(1) and Os(2) atoms with appropriate distance restraints. The disorder found in the solvent molecule in **2c**·CH_2Cl_2 was refined accordingly with distance and similarity restraints. All hydrogen atoms were assigned calculated positions and allowed to ride on the attached carbon atom during data reduction. The X-ray data and processing parameters for the four compounds are reported in Table 1, with selected bond distances and angles for clusters **2** and **3** quoted in Table 2.

2.10. Computational methodology

The DFT calculations reported here were performed with the Gassian09 package of programs [24]. The calculations were carried out with the B3LYP functional, which utilizes the Becke three-parameter exchange functional (B3) [25] combined with the correlation functional of Lee, Yang, and Parr (LYP) [26]. The osmium atoms were described by Stuttgart–Dresden effective core potentials (ecp) and the SDD basis set, while the 6–31G(d′) basis set, as implemented in the Gaussian09 program suite, was employed for

Table 1
X-ray crystallographic data and processing parameters for the ligand dppq and the triosmium clusters **2b**, **2c**·CH_2Cl_2, and **3**·2$CDCl_3$.

Compound	dppq	**2b**	**2c**	**3**
CCDC entry no.	730322	730323	730320	730321
Cryst syst	Triclinic	Triclinic	Triclinic	Triclinic
Space group	P – 1	P – 1	P – 1	P – 1
a, Å	9.373(2)	12.114(1)	10.4813(5)	10.972(2)
b, Å	10.087(2)	12.973(1)	12.4726(6)	12.140(2)
c, Å	14.860(3)	13.706(1)	17.7436(9)	18.592(3)
α, deg	74.249(2)	89.681(1)	94.388(1)	83.210(2)
β, deg	75.552(2)	69.009(1)	106.205(1)	75.021(1)
γ, deg	72.217(2)	86.667(1)	94.191(1)	79.369(1)
V, Å^3	1266.1(4)	2007.2(3)	2210.1(2)	2344.8(6)
Mol formula	$C_{32}H_{24}N_2P_2$	$C_{42}H_{24}N_2O_{10}Os_3P_2$	$C_{43}H_{26}Cl_2N_2O_{10}Os_3P_2$	$C_{43}H_{24}Cl_6D_2N_2O_9Os_3P_2$
fw	498.47	1349.17	1434.10	1561.91
Formula units per cell (Z)	2	2	2	2
D_{calcd} (Mg/m^3)	1.308	2.232	2.155	2.212
λ (Mo Ka), Å	0.71073	0.71073	0.71073	0.71073
Absorption coeff (mm^{-1})	0.196	9.614	8.855	8.575
Abs corr factor	0.9442/0.9404	0.2615/0.1339	0.4755/0.1490	0.6641/0.4840
Total reflections	5641	24,370	27,231	27,210
Independent reflections	5641	8665	9401	9185
Data/res/parameters	5641/0/326	8665/0/532	9401/10/569	9185/2/590
R1[a] ($I \geq 2\sigma(I)$]	0.0535	0.0169	0.0241	0.0367
wR2[b]	0.1328	0.0452	0.0651	0.0515
GOF on F^2	1.133	1.004	1.050	0.996
$\Delta\rho$(max), $\Delta\rho$(min) (e/Å^3)	0.856/−0.614	0.955/−1.487	2.636/−1.824	1.147/−0.882

[a] $R1 = \Sigma||F_o| - |F_c||/\Sigma|F_o|$.
[b] $R2 = \{\Sigma[w(F_o^2 - F_c^2)^2/\Sigma[w(F_o^2)^2]\}^{1/2}$.

Table 2
Selected bond distances (Å) and angles (°) for the triosmium clusters **2b**, **2c**·CH_2Cl_2, and **3**·2$CDCl_3$.

Cluster **2b**			
Bond distances			
Os(1)–P(1)	2.3403(8)	Os(1)–Os(2)	2.8813(3)
Os(1)–Os(3)	2.9097(3)	Os(2)–P(2)	2.3286(8)
Os(2)–Os(3)	2.8638(3)	C(11)–C(12)	1.446(4)
P(1)···P(2)	3.621(1)		
Bond angles			
P(1)–Os(1)–Os(2)	103.13(2)	P(1)–Os(1)–Os(3)	159.18(2)
P(2)–Os(2)–Os(3)	154.21(2)	P(2)–Os(2)–Os(1)	93.67(2)
C(11)–P(1)–Os(1)	115.35(9)	C(12)–P(2)–Os(2)	113.0(1)
Cluster **2c**			
Bond distances			
Os(1)–P(2)	2.299(1)	Os(1)–P(1)	2.299(1)
Os(1)–Os(3)	2.9116(3)	Os(1)–Os(2)	2.9237(3)
Os(2)–Os(3)	2.8983(3)	C(11)–C(12)	1.426(6)
P(1)···P(2)	3.132(1)		
Bond angles			
P(2)–Os(1)–P(1)	85.90(4)	P(2)–Os(1)–Os(2)	163.57(3)
P(1)–Os(1)–Os(2)	108.60(3)	C(11)–P(1)–Os(1)	105.3(1)
C(12)–P(2)–Os(1)	106.5(1)	C(12)–C(11)–P(1)	116.8(3)
C(11)–C(12)–P(2)	117.6(3)		
Cluster **3**			
Bond distances			
Os(1)–Os(3)	2.9300(5)	Os(1)–Os(2)	2.9683(5)
Os(2)–Os(3)	2.8720(5)	Os(1)–H(1)	1.79(6)
Os(2)–H(1)	1.71(6)	Os(1)–P(1)	2.310(2)
Os(1)–P(2)	2.367(2)	Os(2)–C(37)	2.192(8)
C(10)–C(11)	1.419(9)		
Bond angles			
C(1)–Os(1)–P(2)	91.6(2)	C(2)–Os(1)–P(2)	171.7(2)
P(1)–Os(1)–P(2)	85.86(6)	C(1)–Os(1)–Os(3)	88.0(2)
P(1)–Os(1)–Os(2)	115.42(5)	C(5)–Os(2)–C(37)	174.3(3)
C(4)–Os(2)–Os(3)	84.7(2)	C(3)–Os(2)–Os(1)	115.9(2)
C(8)–Os(3)–Os(2)	100.5(2)	C(9)–Os(3)–Os(1)	98.2(2)

the remaining atoms. The geometry-optimized structures reported here represent minima based on zero imaginary frequencies (positive eigenvalues), as established by frequency calculations using the analytical Hessian.

3. Discussion

3.1. Synthesis and X-ray structure of dppq

The synthesis of dppq has recently been reported by Glueck et al. through the CuCl-catalyzed coupling of 2,3-dichloroquinoxaline with Ph_2PH [27,28]. Alternatively, the reaction between 2,3-dichloroquinoxaline and Ph_2PLi, the latter which is prepared *in situ* from BuLi and Ph_2PH, also furnishes the desired diphosphine in high yield as a relatively air-stable, yellow solid. Our procedure makes use of the facile addition-elimination reaction of the nucleophilic Ph_2P^- anion at the chlorine-activated C_2 and C_3 centers of the parent heterocycle [29]. The ^1H and ^{31}P NMR spectroscopic properties of dppq recorded in $CDCl_3$ and C_6D_6 are consistent with the formulated structure. The solid-state structure of dppq was crystallographically determined, and the thermal ellipsoid plot of the molecular structure is shown in Fig. 1, whose caption also contains selected bond distances and angles for dppq. The diphosphine ligand was also examined by DFT calculations, and the geometry-optimized B3LYP structure of dppq is depicted in the right-hand side of Fig. 1. The optimized structure computed for dppq, and with it the basic disposition of the aryl groups associated with the P(1) and P(2) moieties, shows an excellent correspondence with the solid-state structure. This uniformity between experiment and theory is important in terms of the orbital properties to be discussed in connection with the cyclic voltammetric behavior of dppq and the dppq-substituted clusters **2b** and **2c**.

3.2. Synthesis, spectroscopic data, and solid-state structure for ***2b***

Treatment of 1,2-$Os_3(CO)_{10}(MeCN)_2$ (**1**) with dppq in CH_2Cl_2 at room temperature leads to the diphosphine-bridged cluster **2b** as

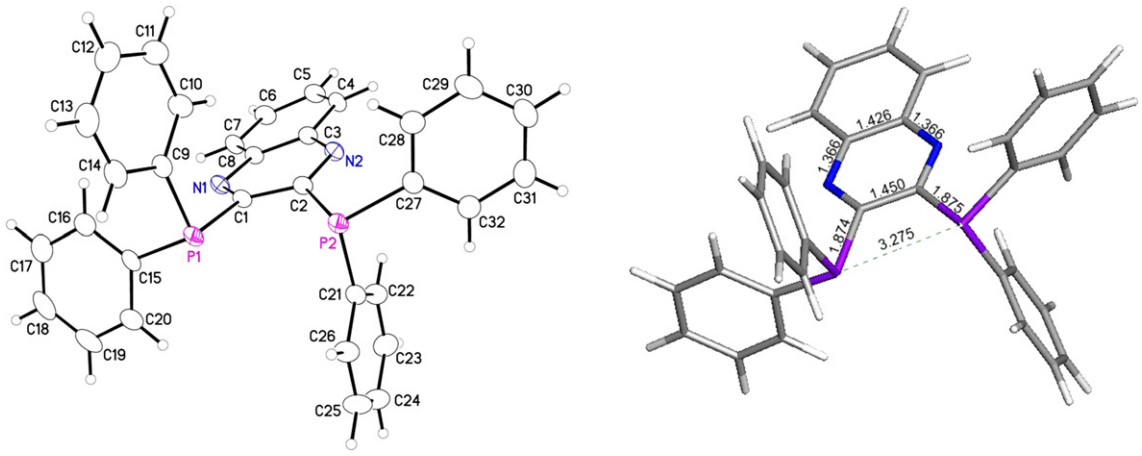

Fig. 1. Thermal ellipsoid plot of the molecular structure of dppq at the 50% probability level (left) and the optimized B3LYP structure of dppq (right). Selected bond distances (Å) and angles (deg) for the X-ray structure: P(1)–C(1) = 1.850(2), P(2)–C(2) = 1.854(2), N(1)–C(1) = 1.310(3), N(1)–C(8) = 1.378(3), N(2)–C(2) = 1.324(3), N(2)–C(3) = 1.373(3), C(1)–C(2) = 1.437(3), P(1)···P(2) = 3.193(2), N(1)–C(1)–P(1) = 119.5(2), C(2)–C(1)–P(1) = 118.1(2), N(2)–C(2)–P(2) = 121.0(2), C(1)–C(2)–P(2) = 117.5(2). The bond distances specified in the B3LYP structure are reported in angstrom.

the sole observable product in 84% isolated yield. **2b** was characterized in solution by IR and NMR spectroscopy, and the recorded high-field singlet in the ^{31}P NMR spectrum at δ 4.41 in C_6D_6 is in full agreement with the bridging of adjacent osmium atoms by the phosphine atoms of the dppq ligand. The formation of **2b** as the kinetically favored substitution product follows the trend displayed by the rigid diphosphine ligands depicted in Scheme 1 and their reaction with cluster **1**. The molecular structure of **2b**, which is shown in Fig. 2, was unequivocally established by X-ray diffraction analysis. The bridging disposition of the dppq ligand and its equatorial coordination to the Os(1) and Os(2) centers are confirmed. The Os–Os bond distances range from 2.8638(3) Å [Os(2)–Os(3)] to 2.9097(3) Å [Os(1)–Os(3)] and are in good agreement with those Os–Os bond distances in the parent cluster $Os_3(CO)_{12}$ and numerous diphosphine-bridged clusters $Os_3(CO)_{10}$(P–P) [2–5,30,31]. The two Os–P bonds display distances of 2.3403(8) Å [Os(1)–P(1)] and 2.3286(8) Å [Os(2)–P(2)], while the ten terminal carbonyl groups exhibit distances and angles consistent with their linear nature. The quinoxaline platform that serves to tether the vicinal Ph_2P moieties is tipped up out of the plane defined by three osmium atoms based on a fold angle of 54.35(5)°. Coordination of the dppq ligand across the Os(1)–Os(2) vector is accompanied by a significant "stretching" of the dppq ligand and an overall ground-state destabilization of cluster **2b** relative to the chelating isomer **2c**. Here the internuclear P(1)···P(2) distance of 3.621(1) Å found in **2b** is significantly longer (ca. >0.40 Å) than the corresponding P(1)···P(2) distance found in free dppq and the chelated cluster **2c**. This perturbation serves as the driving force for the isomerization of **2b** to **2c** (*vide supra*), paralleling the isomerization behavior of the diphosphine ligands depicted in Scheme 1. Moreover, the theoretical underpinning for the isomerization of the P–P ligand in $Os(CO)_{10}$(P–P) clusters has been thoroughly examined by us as a function of the diphosphine ligand [7]. The B3LYP optimized structure of **2b** is depicted in Fig. 2, and apart from the enhanced D_3 twist of the axial CO groups relative to the metallic plane and the slightly elongated internuclear P(1)···P(2), it is in qualitative agreement with the crystallographic structure.

3.3. Isomerization kinetics of *2b* to *2c*

Numerous reports now exist on the non-dissociative, bridge-to-chelate isomerization of the ancillary diphosphine in $Os(CO)_{10}$(P–P) clusters [2–5,7,32]. Naturally, this led us to examine the thermal stability of **2b** in order to establish the influence of the dppq ligand on

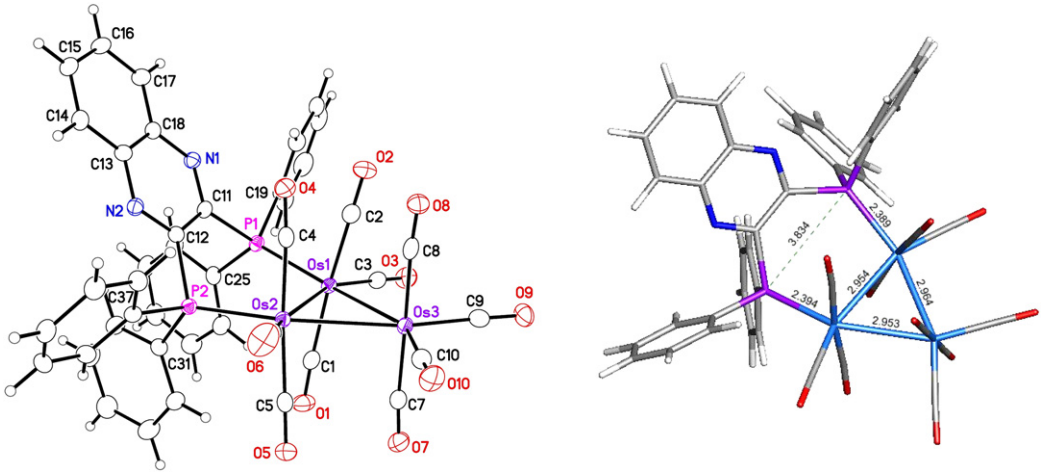

Fig. 2. Thermal ellipsoid plot of the molecular structure of **2b** (left; at the 50% probability level) and the optimized B3LYP structure of **2b** (right). The bond distances specified in the B3LYP structure are reported in angstrom.

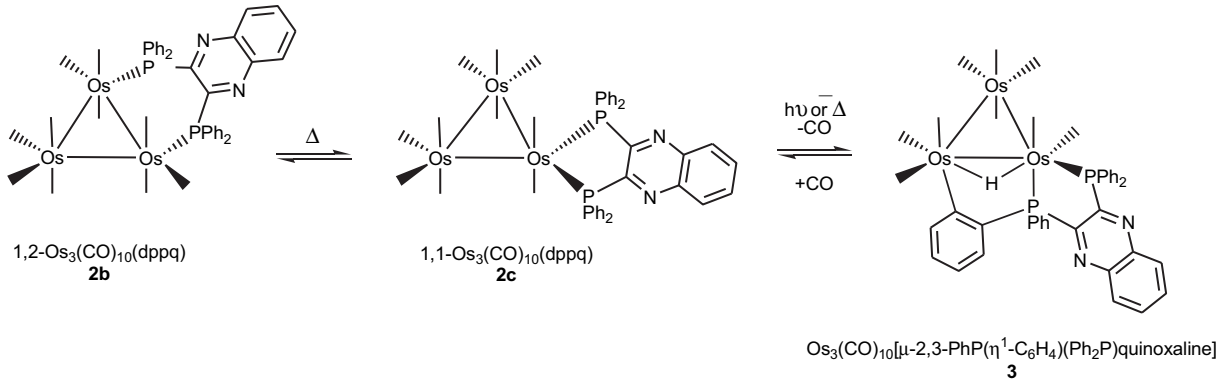

1,2-$Os_3(CO)_{10}$(dppq)
2b

1,1-$Os_3(CO)_{10}$(dppq)
2c

$Os_3(CO)_{10}$[μ-2,3-PhP(η^1-C_6H_4)(Ph_2P)quinoxaline]
3

Scheme 2.

the isomerization reaction. When heated under CO, **2b** isomerizes cleanly to **2c** and this confirms that the latter cluster is the thermodynamically more stable form of $Os(CO)_{10}$(dppq). The addition of CO suppresses the formation of the hydride cluster **3**, but CO addition has been shown not to affect the equilibrium for the bridged-to-chelated ligand isomerization in other decacarbonyl clusters $Os_3(CO)_{10}$(P–P) examined by our group [2–5,7,32]. Scheme 2 illustrates this isomerization and the fate of the unsaturated intermediate, $Os_3(CO)_9$(dppq) (not shown), that forms from decarbonylation of **2c** and which functions as the precursor to the hydride cluster **3**.

Cluster **2c** was isolated by column chromatography, characterized in solution by traditional spectroscopic methods, and the molecular structure determined by X-ray diffraction analysis. The singlet recorded at δ 13.20 in C_6D_6 in the ^{31}P NMR spectrum of **2c** is in full agreement with a triosmium cluster possessing a chelating dppq ligand. The large nuclear deshielding in the ^{31}P resonance that accompanies the bridge-to-chelate isomerization is a diagnostic feature of such a reaction [33]. Fig. 3 shows the thermal ellipsoid plot of the molecular structure of **2c**, as the CH_2Cl_2 solvate, and confirms the attendant isomerization of the dppq ligand upon heating. The Os–Os bond distances range from 2.8983(3) Å [Os(2)–Os(3)] to 2.9237(3) Å [Os(1)–Os(2)]. The internuclear P(1)···P(2) distance of 3.132(1) Å has undergone a significant contraction, relative to that distance found in **2b**, and the angles associated with the Os(1)–P(1)–C(11) [105.3(1)°], Os(1)–P(2)–C(12) [106.5(1)°], C(12)–C(11)–P(1) [116.8(3)°], and C(11)–C(12)–P(2) [117.6(3)°] linkages display values that are in excellent agreement with the idealized hybridization state of the subtended atom. The observed angle of 85.90(4)° for the P(1)–Os(1)–P(2) atoms is in keeping with the chelating nature of the ancillary dppq ligand. The DFT structure computed for **2c** that is depicted in Fig. 3 shows a good correspondence with the diffraction structure. Here the computed bond distances and angles, and the orientation of the phenyl groups at the P(1) and P(2) atoms closely match the crystallographic values and disposition of the ancillary ligands. The DFT calculations on the isomeric $Os_3(CO)_{10}$(dppq) clusters confirm the greater stability of dppq-chelated species vis-à-vis the bridging isomer **2b**. Here **2c** is computed to have a 4.8 kcal/mol lower free energy than **2b**, which translates to a $K_{eq} > 3300$ in favor of **2c** [34]; this finding is in keeping with our recent calculations on a series of diphosphine-substituted $Os_3(CO)_{10}$(P–P) clusters [7].

The **2b** → **2c** isomerization was investigated kinetically by NMR spectroscopy under CO, over the temperature range 323–353 K. The first-order rate constants are given in Table 3. The progress of these reactions was easily monitored by following the concentration changes in either the ^{31}P singlet or ^{1}H resonances associated with **2b** as a function of time. The Eyring plot of these data is shown in Fig. 4, and the Eyring activation parameters [$\Delta H^{\neq} = 25.4(4)$ kcal/mol; $\Delta S^{\neq} = -3(1)$ eu] parallel those data reported by us for related ligand isomerizations (Table 4), whose intramolecular isomerization involves the "merry-go-round" migration of phosphine and CO groups about the cluster polyhedron.

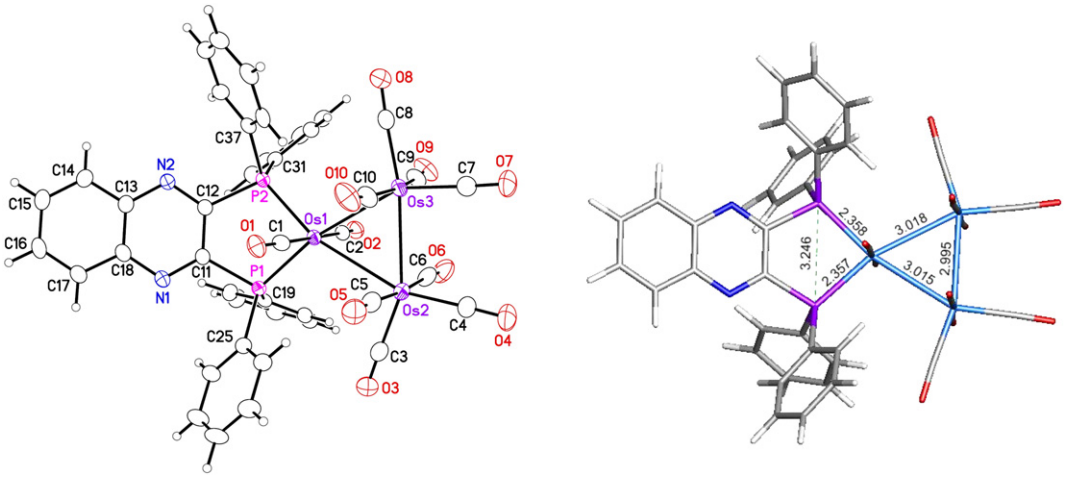

Fig. 3. Thermal ellipsoid plot of the molecular structure of **2c** (left; at the 50% probability level) and the optimized B3LYP structure of **2c** (right). The CH_2Cl_2 solvent molecule in the X-ray diffraction structure has been omitted for clarity, and the bond distances specified in the B3LYP structure are reported in angstrom.

Table 3
Experimental rate constants for the isomerization of 1,2-$Os_3(CO)_{10}$(dppq) to 1,1-$Os_3(CO)_{10}$(dppq) under CO.[a]

Entry	Temp (K)	10^6k (s^{-1})
1	323.0	2.25(2)
2	333.0	8.9(1)
3	343.0	26.2(4)[b]
4	353.0	73(2)

[a] The ^{31}P NMR kinetic data were collected in $CDCl_3$ solvent using a ca. 10^{-2} M solution of starting cluster by following the change in the ^{31}P resonances for the bridging and chelating isomers of $Os_3(CO)_{10}$(dppq). All NMR reactions were performed under 1 atm CO.
[b] ^{1}H NMR reaction conducted in $CDCl_3$ using a ca. 10^{-2} M of starting cluster in the presence of Cp_2Fe (internal standard).

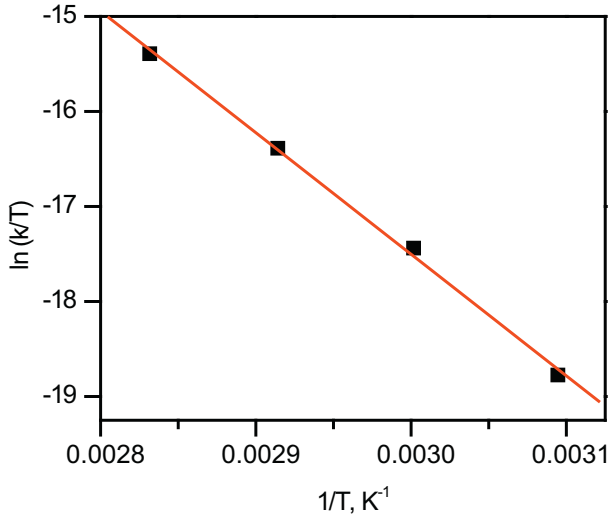

Fig. 4. Eyring plot for the conversion of **2b** → **2c** over the temperature range of 323–353 K.

3.4. Reversible ortho metalation in *2c* and formation of $HOs_3(CO)_9[\mu$-2,3-PhP(η^1-C_6H_4)(Ph_2P)quinoxaline] (*3*)

The reactivity of **2c** was next examined as part of our ongoing interest in ligand activation processes associated with cluster-coordinated ligands [1f,2–5,7,32,35]. **2c** is stable to CO loss at temperatures below 333 K, but is sensitive to near-UV irradiation (366 nm). Photolysis of a toluene solution containing **2c** leads to CO loss and formation of **3**. The hydride-bridged cluster **3** was obtained in high yield and without complications by simply purging the reaction solution during photolysis, using nitrogen or argon to remove the liberated CO. Alternatively, CO removal through several freeze–pump–degas cycles during the course of the irradiation also furnishes **3** in comparable yield. This particular reaction is particularly sensitive to extraneous CO, and treatment of **3** with added CO at 333 K regenerates **2c** in quantitative yield. This latter experiment establishes the reversible nature of the ortho metalation of the ancillary dppq ligand.

3 was isolated in 88% yield after purification by column chromatography, followed by recrystallization. The bridging hydride recorded at δ −15.84 in the ^{1}H NMR spectrum (in C_6D_6) and the pair of inequivalent doublets recorded at δ 13.60 and 17.58 in the ^{31}P NMR spectrum are in keeping with the formulated structure of **3**. Fig. 5 shows the thermal ellipsoid plot of the molecular structure of **3**, as the bis-$CDCl_3$ solvate, and confirms the ortho metalation of one of the aryl rings of the dppq ligand. **3** contains 48e and is electronically saturated, assuming that the ortho-metalated dppq ligand functions as a 5e donor group. The Os–Os bond lengths range from 2.8720(5) Å [Os(2)–Os(3)] to 2.9683(5) Å [Os(1)–Os(2)], with the latter Os–Os vector serving as the locus of the bridging hydride ligand [36]. The stereochemical disposition of the C(3)O(3) and P(1) groups about the cluster polyhedron further supports our contention concerning the location of the hydride. Here the Os(1)–Os(2)–C(3) and Os(2)–Os(1)–P(1) angles of 115.9(2) and 115.42(5)°, respectively, are significantly expanded from the idealized value of ca. 90° typically found for equatorial substituents at triangular clusters due to the presence of the ancillary hydride [37,38]. Both phosphine atoms are coordinated to the Os(1) center and display axial [P(2)] and equatorial [P(1)] dispositions. The Os(2)–C(37) bond distance of 2.192(8) Å is comparable to the Os–C bond distance found in the triosmium clusters $H_2Os_3(CO)_9(\mu$-$C_6H_4PPh)$, $HOs_3(CO)_9(PPh_3)(\mu$-$SbPh_2)(\mu$-$C_6H_4)$, and $Os_3(CO)_9[\mu$-$PPh(C_6H_4)CH_2PPh]$, each of which possesses an activated aryl moiety [39].

3.5. Redox behavior and MO properties of the HOMO and LUMO levels in dppq and clusters *2b* and *2c*

The redox properties of the dppq ligand and the isomeric clusters $Os_3(CO)_{10}$(dppq) were examined by cyclic voltammetry (CV) in CH_2Cl_2 containing 0.2 M TBAP as the supporting electrolyte. The CV of dppq recorded over the potential range of 1.4 V to −1.6 V and at a scan rate of 250 mV/s revealed a diffusion-controlled, one-electron reduction at $E_{1/2} = -1.66$ V [40]. Employing the electrochemical assignments of Kaim for the R,R-2,3-bis(*tert*-butylmethylphosphino)quinoxaline ligand, the site of the $0/1^-$ redox couple in dppq is readily ascribed to quinoxaline platform [11]. A single, irreversible oxidation at $E_p^a = 1.03$ was also found, and this wave remained irreversible under all conditions explored (scan rates up to 1.0 V/s and temperatures down to 243 K). The

Table 4
Summary of the Eyring activation data for the bridge-to-chelate isomerization of different diphosphine ligands in the triosmium clusters $Os_3(CO)_{10}$(P–P).

Ligand	$\Delta H^{\neq}$ (kcal/mol)	$\Delta S^{\neq}$ (eu)	Ref
dppen[a]	26.5(6)	−5(2)	[2]
bpcd	25.0(7)	−2(2)	[3]
bmi	24.0(1)	−5(1)	[4]
fbpcd	23.1(3)	−7(1)	[5]
dppbz	21.6(3)	−11(1)	[7]
bmf[a]	26.9(7)	6(1)	Unpublished
dppq	25.4(4)	−3(1)	This work

[a] The isomerization is reversible and only the activation parameters for the forward portion of the reaction are reported.

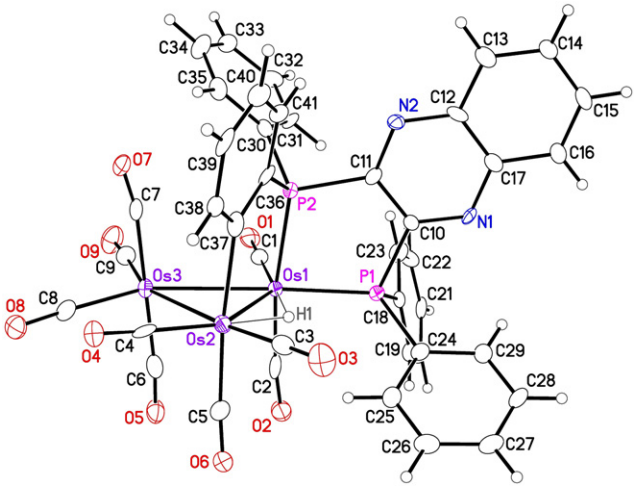

Fig. 5. Thermal ellipsoid plot of the molecular structure of **3** at the 50% probability level. The $CDCl_3$ solvent molecules have been omitted for clarity.

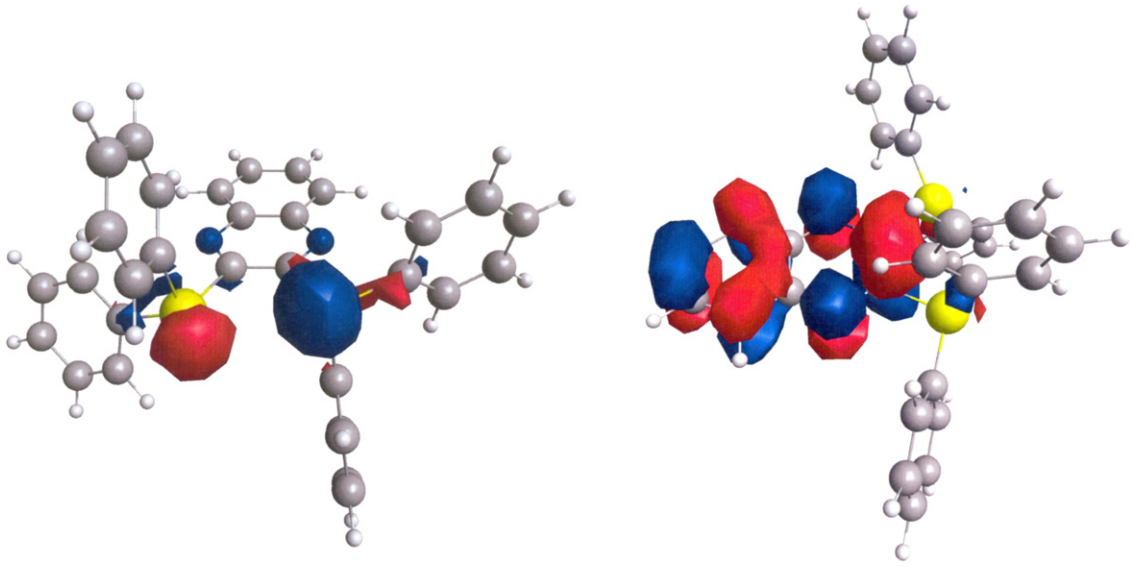

Fig. 6. Contour plots of the HOMO (left) and LUMO (right) for dppq.

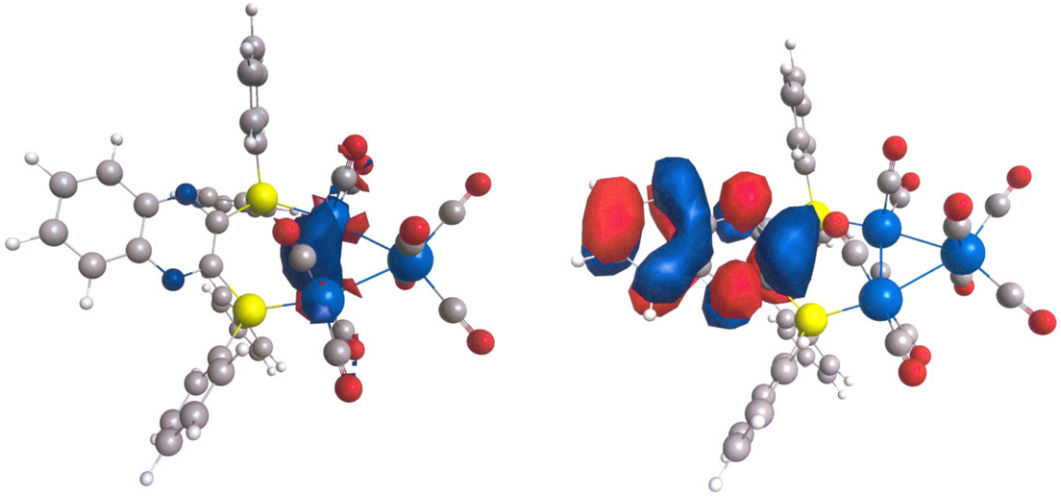

Fig. 7. Contour plots of the HOMO (left) and LUMO (right) for **2b**.

orbital composition of the HOMO and LUMO levels in dppq was addressed through DFT analysis, using the optimized structure for dppq. As seen in the contour diagrams in Fig. 6, the π^* LUMO is localized almost exclusively on the heterocyclic platform, while the principal contribution to the HOMO is best viewed as originating from the out-of-phase combination involving the lone-electron pair orbital at each phosphorus atom.

The CV of **2b** was recorded in CH_2Cl_2 under conditions similar to those described above for dppq. A reversible, one-electron reduction ($E_{1/2} = -1.72$ V) and an irreversible, multielectron oxidation ($E_p^a = 0.52$) were found for **2b**. While electron accession at the heterocyclic ring of the bridging dppq ligand accounts for the $0/1^-$ redox process, the observed cathode shift in the E_p^a wave is inconsistent with an dppq-based oxidation. Coordination of the dppq ligand to the Os_3 frame in **2b** is expected to an anodic shift in the redox potential of the energy of the out-of-phase lone-electron pair (i.e., the HOMO of the free ligand), as demonstrated by Kaim for different mononuclear Quinox-P-substituted derivatives [11]. Phosphine substitution at metal clusters has been shown to raise the energy of metal-based orbitals, especially metal–metal bonding orbitals [41]. Accordingly, the oxidation in **2b** is ascribed to an oxidation of an Os–Os bonding orbital, one with little or no dppq character. Our redox assignments for **2b** were validated by DFT analysis of the HOMO and LUMO levels, whose contour plots are depicted in Fig. 7.

Isomerization of the dppq ligand in **2b** does not lead to significant changes in the redox properties of **2c**. Apart from the minor potential differences in the reversible reduction ($E_{1/2} = -1.62$) and the irreversible oxidation ($E_p^a = 0.34$), the recorded CV of **2c** is unexceptional relative to that found for **2b**; the DFT computed HOMO and LUMO levels for **2c** (not shown) follow suit and warrant no further comment.

4. Conclusions

Replacement of the MeCN ligands in 1,2-$Os_3(CO)_{10}(MeCN)_2$ by the diphosphine ligand dppq furnishes 1,2-$Os_3(CO)_{10}$(dppq) as the kinetic product of ligand substitution. The dppq ligand in 1,2-$Os_3(CO)_{10}$(dppq) is coordinatively flexible and readily isomerizes under CO (1 atm) over the temperature range of 323–353 K to

furnish 1,1-$Os_3(CO)_{10}$(dppq) in quantitative yield. The ground-state energy difference between the kinetic and thermodynamic forms of $Os_3(CO)_{10}$(dppq) has been evaluated by DFT calculations, and the computed energy difference is in concert with the experimental data. The redox properties of the free ligand and the decacarbonyl products were investigated by cyclic voltammetry, and the LUMO in all three compounds was found to be localized on the quinoxaline platform, as verified by DFT calculations. Future studies will probe the electrochemical behavior of different $Os_3(CO)_{10}$(P-P) clusters that contain a redox-active P–P auxiliary, one whose potential is tunable as a function of the ancillary substituents and heterocyclic architecture.

Acknowledgment

Financial support from the Robert A. Welch Foundation (Grant B-1093-MGR) is greatly appreciated, and X. Wang acknowledges support by the U.S. Department of Energy, Office of Science, under Contract No. DE-AC05-00OR22725 managed by UT Battelle, LLC. NSF support of the NMR and computational facilities at UNT through grants CHE-0840518 and CHE-0741936 is acknowledged. We also wish to thank Prof. Michael B. Hall (TAMU) for providing us a copy of his *JIMP2* program, which was used to prepare the geometry-optimized structures reported here, and Dr. David A. Hrovat (Center for Advanced Scientific Computing and Modeling, UNT) for his assistance and guidance with computational aspects for this work.

Appendix A. Supporting information

CCDC 730322, 730323, 730320, and 730321 contain the supplementary crystallographic data for the ligand dppq and the triosmium clusters **2b**, **2c**, and **3**, respectively. These data can be obtained free of charge from The Cambridge Crystallographic Data Center via http://www.ccdc.cam.ac.uk/data_request/cif.

References

[1] (a) A.J. Deeming, S. Donovan-Mtunzi, S.E. Kabir, J. Organomet. Chem. 276 (1984) C65;
(b) A.J. Deeming, S.E. Kabir, J. Organomet. Chem. 340 (1988) 359;
(c) A.J. Deeming, S. Donovan-Mtunzi, K.I. Hardcastle, S.E. Kabir, K. Henrick, M. McPartlin, J. Chem. Soc., Dalton Trans. (1988) 579;
(d) S.E. Kabir, A. Miah, L. Nesa, K. Uddin, K.I. Hardcastle, E. Rosenberg, A.J. Deeming, J. Organomet. Chem. 492 (1995) 41;
(e) N. Begum, U.K. Das, M. Hassan, G. Hogarth, S.E. Kabir, E. Nordlander, M.A. Rahman, D.A. Tocher, Organometallics 26 (2007) 6462;
(f) S.-H. Huang, J.M. Keith, M.B. Hall, M.G. Richmond, Organometallics 29 (2010) 4041.
[2] W.H. Watson, G. Wu, M.G. Richmond, Organometallics 24 (2005) 5431.
[3] W.H. Watson, G. Wu, M.G. Richmond, Organometallics 25 (2006) 930.
[4] W.H. Watson, B. Poola, M.G. Richmond, J. Organomet. Chem. 691 (2006) 4676.
[5] W.H. Watson, B. Poola, M.G. Richmond, Polyhedron 26 (2007) 3585.
[6] For a related report that describes the bridge-to-chelate isomerization of a thiophosphine at a triosmium cluster, see: R. Persson, M. Monari, R. Gobetto, A. Russo, S. Aime, M.J. Calhorda, E. Nordlander Organometallics 20 (2001) 4150.
[7] X. Zhang, S. Kandala, L. Yang, W.H. Watson, X. Wang, D.A. Hrovat, W.T. Borden, M.G. Richmond, Organometallics 30, (2011), in press.
[8] F.A. Cotton, Inorg. Chem. 5 (1966) 1083.
[9] T. Imamoto, K. Sugita, K. Yoshida, J. Am. Chem. Soc. 127 (2005) 11934.
[10] For reports of asymmetric hydrogenation and hydroformylation using chiral QuinoxP and QuinoxP-related ligands, see: (a) T. Imamoto, T. Itoh, Y. Yamanoi, R. Narui, K. Yoshida, Tetrahedron: Asymmetry 17 (2006) 560;
(b) T. Imamoto, A. Kumada, H. Yoshida, Chem. Lett. 36 (2007) 500.
(c) T. Imamoto, M. Nishimura, A. Koide, K. Yoshida, J. Org. Chem. 72 (2007) 7413;
(d) A.T. Axtell, J. Klosin, G.T. Whiteker, C.J. Cobley, M.E. Fox, M. Jackson, K.A. Abboud, Organometallics 28 (2009) 2993;
(e) M.E. Fox, M. Jackson, I.C. Lennon, J. Klosin, K.A. Kbboud, J. Org. Chem. 73 (2008) 775.
[11] A.K. Das, E. Bulak, B. Sarkar, F. Lissner, T. Schleid, M. Niemeyer, J. Fiedler, W. Kaim, Organometallics 27 (2008) 218.
[12] J.N. Nicholls, M.D. Vargas, Inorg. Synth. 26 (1989) 289.
[13] S.R. Drake, P.A. Loveday, Inorg. Synth. 28 (1990) 230.
[14] W.G. Kofron, L.M. Baclawski, J. Org. Chem. 41 (1976) 1879.
[15] D.F. Shriver, The Manipulation of Air-Sensitive Compounds. McGraw-Hill, New York, 1969.
[16] We have arbitrarily assigned the shielded portion of quinoxaline ^{1}H spin system as belonging to the AA′ hydrogens. The $J_{AA'}$ coupling constant was computed to be 0.8 Hz.
[17] B.K. Carpenter, Determination of Organic Reaction Mechanisms. Wiley-Interscience, New York, 1984.
[18] A.J. Bard, L.R. Faulkner, Electrochemical Methods: Fundamentals and Applications, second ed. Wiley, New York, 2001.
[19] APEX2 Version 2.14. Bruker AXS Inc, Madison, WI, 2007.
[20] G.M. Sheldrick, Acta Cryst. A64 (2008) 112.
[21] A.L. Spek, J. Appl. Cryst. 36 (2003) 7.
[22] Bruker SADABS. Bruker AXS Inc., Madison, WI, 2007.
[23] A.G. Orpen, Dalton Trans. (1980) 2509.
[24] M.J. Frisch, G.W. Trucks, H.B. Schlegel, G.E. Scuseria, M.A. Robb, J.R. Cheeseman, G. Scalmani, V. Barone, B. Mennucci, G.A. Petersson, H. Nakatsuji, M. Caricato, X. Li, H.P. Hratchian, A.F. Izmaylov, J. Bloino, G. Zheng, J.L. Sonnenberg, M. Hada, M. Ehara, K. Toyota, R. Fukuda, J. Hasegawa, M. Ishida, T. Nakajima, Y. Honda, O. Kitao, H. Nakai, T. Vreven, J.A. Montgomery Jr., J.E. Peralta, F. Ogliaro, M. Bearpark, J.J. Heyd, E. Brothers, K.N. Kudin, V.N. Staroverov, R. Kobayashi, J. Normand, K. Raghavachari, A. Rendell, J.C. Burant, S.S. Iyengar, J. Tomasi, M. Cossi, N. Rega, J.M. Millam, M. Klene, J.E. Knox, J.B. Cross, V. Bakken, C. Adamo, J. Jaramillo, R. Gomperts, R.E. Stratmann, O. Yazyev, A.J. Austin, R. Cammi, C. Pomelli, J.W. Ochterski, R.L. Martin, K. Morokuma, V.G. Zakrzewski, G.A. Voth, P. Salvador, J.J. Dannenberg, S. Dapprich, A.D. Daniels, O. Farkas, J.B. Foresman, J.V. Ortiz, J. Cioslowski, D.J. Fox, Gaussian 09, Revision A.02. Gaussian, Inc., Wallingford, CT, 2009.
[25] A.D. Becke, J. Chem. Phys. 98 (1993) 5648.
[26] C. Lee, W. Yang, R.G. Parr, Phys. Rev. B 37 (1988) 785.
[27] M.F. Cain, S.C. Reynolds, D.S. Glueck, J.A. James, A.L. Rheingold, ACS National Meeting, Boston, MA, 2010, INOR-561.
[28] For a report on the synthesis and coordination chemistry of the phosphine oxide based on dppq, see: E.I. Matrosov, Z.A. Starikova, A.A. Khodak, E.E. Nifant'ev Zh. Neorg. Khim. 48 (2003) 2008.
[29] T.L. Gilchrist, Heterocyclic Chemistry, third ed. Addison Wesley Longman, Essex, UK, 1997.
[30] (a) E.R. Corey, L.F. Dahl, Inorg. Chem. 1 (1962) 521;
(b) M.R. Churchill, B.G. DeBoer, Inorg. Chem. 16 (1977) 878.
[31] (a) J.A. Clucas, R.H. Dawson, P.A. Dolby, M.M. Harding, K. Pearson, A.K. Smith, J. Organomet. Chem. 311 (1986) 153;
(b) W.H. Watson, B. Poola, M.G. Richmond, J. Chem. Crystallogr. 36 (2006) 123;
(c) V. Nesterov, B. Poola, X. Wang, M.G. Richmond, J. Organomet. Chem. 692 (2007) 1806;
(d) K.A. Azam, M.B. Hursthouse, S.E. Kabir, K.M. Abdul Malik, M.A. Mottalib, J. Chem. Crystallogr. 29 (1999) 813.
[32] S. Kandala, L. Yang, C.F. Campana, V. Nesterov, X. Wang, M.G. Richmond, Polyhedron 29 (2010) 2814.
[33] P.E. Garrou, Chem. Rev. 81 (1981) 229.
[34] The ΔE and ΔH (at 298 K) values for the equilibrium between **2b** and **2c** are computed as −3.3 kcal/mol and −3.2 kcal/mol, respectively.
[35] (a) B. Poola, C.J. Carrano, M.G. Richmond, Organometallics 27 (2008) 3018;
(b) S. Kandala, C. Hammons, W.H. Watson, X. Wang, M.G. Richmond, Dalton Trans. 39 (2010) 1620.
[36] D.M.P. Mingos, D.J. Wales, Introduction to Cluster Chemistry. Prentice Hall, Englewood Cliffs, NJ, 1990.
[37] (a) M.R. Churchill, F.J. Hollander, R.A. Lashewycz, G.A. Pearson, J.R. Shapley, J. Am. Chem. Soc. 103 (1981) 2430;
(b) M.R. Churchill, F.J. Hollander, Inorg. Chem. 20 (1981) 4124.
[38] The angular perturbation induced by the hydride on the mutually *cis* C(3)O(3) and P(1) ligands may be contrasted with the average angle of 92.9° found for the four other equatorial groups [C(1)–Os(1)–Os(3), C(4)–Os(2)–Os(3), C(8)–Os(3)–Os(2), and C(9)–Os(3)–Os(1)] in **3**.
[39] (a) S.B. Colbran, P.T. Irele, B.F.G. Johnson, F.J. Lahoz, J. Lewis, P.R. Raithby, Dalton Trans. (1989) 2023;
(b) G. Chen, M. Deng, C.K. Lee, W.K. Leong, Organometallics 21 (2002) 1227;
(c) S.E. Kabir, M.A. Miah, N.C. Sarker, G.M.G. Hussain, K.I. Hardcastle, E. Nordlander, E. Rosenberg, Organometallics 24 (2005) 3315.
[40] Electrochemical reversibility and electron stoichiometry were determined via the usual methods, see P.H. Rieger, Electrochemistry. Chapman and Hall, New York, 1994.
[41] (a) A.M. Bond, P.A. Dawson, B.M. Peake, P.H. Rieger, B.H. Robinson, J. Simpson, Inorg. Chem. 18 (1979) 1413;
(b) M. Arewgoda, P.H. Rieger, B.H. Robinson, J. Simpson, S.J. Visco, J. Am. Chem. Soc. 104 (1982) 5633;
(c) M.G. Richmond, J.K. Kochi, Inorg. Chem. 25 (1986) 656;
(d) A.J. Downard, B.H. Robinson, J. Simpson, Organometallics 5 (1986) 1132.